Journal of Environmental Management 381 (2025) 125157

Contents lists available at ScienceDirect

Journal of Environmental Management

journal homepage: www.elsevier.com/locate/jenvman

Research article

Comparative analysis of evapotranspiration and water yield in basins of the Northern Gulf of America between the past and next 40 years

Ying Ouyang

USDA Forest Service, Southern Research Station, Center for Bottomland Hardwoods Research, 775 Stone Blvd., Thompson Hall, Room 309, Mississippi State, MS, 39762, USA

ARTICLE INFO

Handling editor: Jason Michael Evans

Keywords:
Weather variation
Evapotranspiration
HAWQS model
Northern Gulf of America
Water yield

ABSTRACT

The Northern Gulf of America (NGOA, formerly known as Northern Gulf of Mexico) is a key economic region for seafood production, recreation, and marine transportation. This study compared evapotranspiration (ET) and water yield in the Sabine River Basin (SRB) and Pearl River Basin (PRB) along the NGOA, focusing on coastal watersheds between two 40-year weather scenarios: past (1985–2024) and future (2025–2064). The analysis was conducted using the HAWQS (Hydrologic and Water Quality System) model, along with Mann-Kendall (M-K) and Kolmogorov-Smirnov (K-S) tests. Simulations showed a two-month shift in the timing of maximum monthly water yield, moving from January in the past scenario to March in the future scenario at the coastal watersheds. Monthly water yield was closely correlated to monthly precipitation, indicating that precipitation played a crucial role in producing water yield. Seasonal ET was roughly twice as high in spring and summer compared to fall and winter, while seasonal water yield was about twice as large in spring and winter compared to fall and summer. Future annual ET at the coastal watersheds were moderately or slightly higher than that of the past, while both the past and future annual ETs were lower in the northernmost (inland) watersheds than in the southernmost (coastal) watersheds. Overall, impacts of weather variation on ET and water yield varied among basins in the NGOA. These findings offer valuable insights to water resource managers, helping them make more informed decisions to mitigate water evaporative losses and increase water yield in coastal watersheds of the NGOA and the similar conditions around the world.

1. Introduction

Human activities and weather variation have become critical factors affecting water supply, conservation, and sustainability in the U.S. and around the world. Over the past several decades, extensive use of surface and ground water resources for agricultural, industrial, and domestic purposes has led to the overdrafts of water resources, causing a noticeable decline. This decline is expected to worsen in the near future (Scanlon et al., 2023). Key hydrological processes such as evapotranspiration (ET) and water yield are crucial for estimating water resources availability and sustainability. Evapotranspiration, which involves both plant leaf water transpiration and surface water evaporation, represents the largest water loss from Earth's surface and is a vital component of the hydrological cycle (Allen et al., 1989; Oren et al., 1998; Ouyang, 2021). Over the past few decades, both hydrological and plant physiological methods have been used to estimate ET. The hydrological approach includes techniques like soil water balance, lysimeters, energy balance, Bowen ratio, aerodynamic methods, and eddy covariance. The plant physiological approach uses methods such as sap flow and chamber systems (Allen et al., 1989; Fisher and Pringle III, 2013; Monteith, 1965; Wullschleger et al., 1998). Recently, remote sensing and machine learning techniques have become increasingly popular for estimating ET (Cemek et al., 2023; Mokhtari et al., 2023; Ouyang et al., 2024).

Water yield refers to the total amount of water from surface runoff, lateral flow and groundwater recharge minus the water lost through ET and soil storage (Oren et al., 1998; Ouyang, 2021). It is often calculated as the difference between precipitation and ET within a watershed, assuming no significant changes in soil water storage over a year. Water yield can be directly measured by dividing the annual streamflow by the watershed area, or it can be estimated using a water budget approach that accounts for soil moisture, precipitation, and potential ET (McKee et al., 2004). Understanding water yield is important for assessing interactions between surface and groundwater, as well as the effects of land use and weather variation on water resources.

While weather variation is a natural process, human activities have

E-mail address: ying.ouyang@usda.gov.

https://doi.org/10.1016/j.jenvman.2025.125157
Received 30 November 2024; Received in revised form 28 February 2025; Accepted 25 March 2025
Available online 3 April 2025
0301-4797/Published by Elsevier Ltd.

accelerated it, causing abnormal weather patterns (Sippel et al., 2020). Weather variation affects water resources by altering precipitation patterns and shifting wet and dry seasons, and results in more extreme weather, such as unusually cold or warm seasons, stronger storms, floods, and droughts in certain years (Keller et al., 2023; Trenberth, 2011). These changes impact ET, streamflow, runoff, snowmelt, groundwater recharge, and overall water yield in watersheds (Gizaw et al., 2017; Jones and Perkins, 2010; Keller et al., 2023; Tripathi et al., 2014; Walker et al., 2011).

The northern Gulf of America (NGOA) (formerly known as northern Gulf of Mexico) plays a key economic role, known for its seafood markets, recreational fishing, beach tourism, and international maritime hub (McKinney et al., 2021). However, it also faces significant environmental challenges and is one of the most impacted coastal regions in the world, home to the largest and most severe hypoxic zone (<2 mg of dissolved O_2/L) in the western Atlantic Ocean (Turner and Rabalais, 2019; Wang and Justic, 2009; Xu and Xu, 2018). From the 1950s to the 1970s, widespread clear-cutting of bottomland hardwood forests in the lower Mississippi River basin adjacent to the NGOA, primarily for crop production, flood control and floodplain development, led to major environmental changes (MacDonald et al., 1979). These and other human activities have caused fluctuations in seasonal and annual streamflow (Xu and Wu, 2006), increased nutrient and sediment loads (Ouyang et al., 2023; Turner et al., 2007), and the expansion of hypoxic zone (Rabalais et al., 2007) in the NGOA.

The hydrological processes such as stream flow, ET, flood, and water yield in the GOA (Gulf of America) have received considerable interest because they have potential adverse ecological, environmental, and economic impacts and implications (Judd, 1995). Liu et al. (2013) investigated spatial and temporal variations of ET and runoff in drainage basins of the GOA during 1901–2008 using the dynamic land ecosystem model (DLEM). They found a significant decreasing trend in ET and an insignificant trend in runoff, precipitation, and stream flow for the entire study area. Particularly, they reported that ET and runoff decreased in the west part but increased in the east part of the study area over the last 108 years. Despite these studies have been made to investigate hydrological processes in the watersheds along the GOA, limited efforts have been devoted to comparing the past and future trends of ET and water yield in coastal watersheds of the NGOA under a changing weather. Knowledge of these phenomena is critical to assess impacts of weather variation on water resources availability and sustainability.

This study aims to conduct a comparative analysis of watershed-scale ET and water yield in the NGOA between the past 40 years (1985–2024) and future 40 years (2025–2064) scenarios. The analysis uses the Hydrologic and Water Quality System (HAWQS) model and multivariate statistical analysis. The study focuses on two key river basins along the NGOA, namely the Sabine River Basin (SRB) in Texas and Louisiana and Pearl River Basin (PRB) in Mississippi and Louisiana (Fig. 1). The

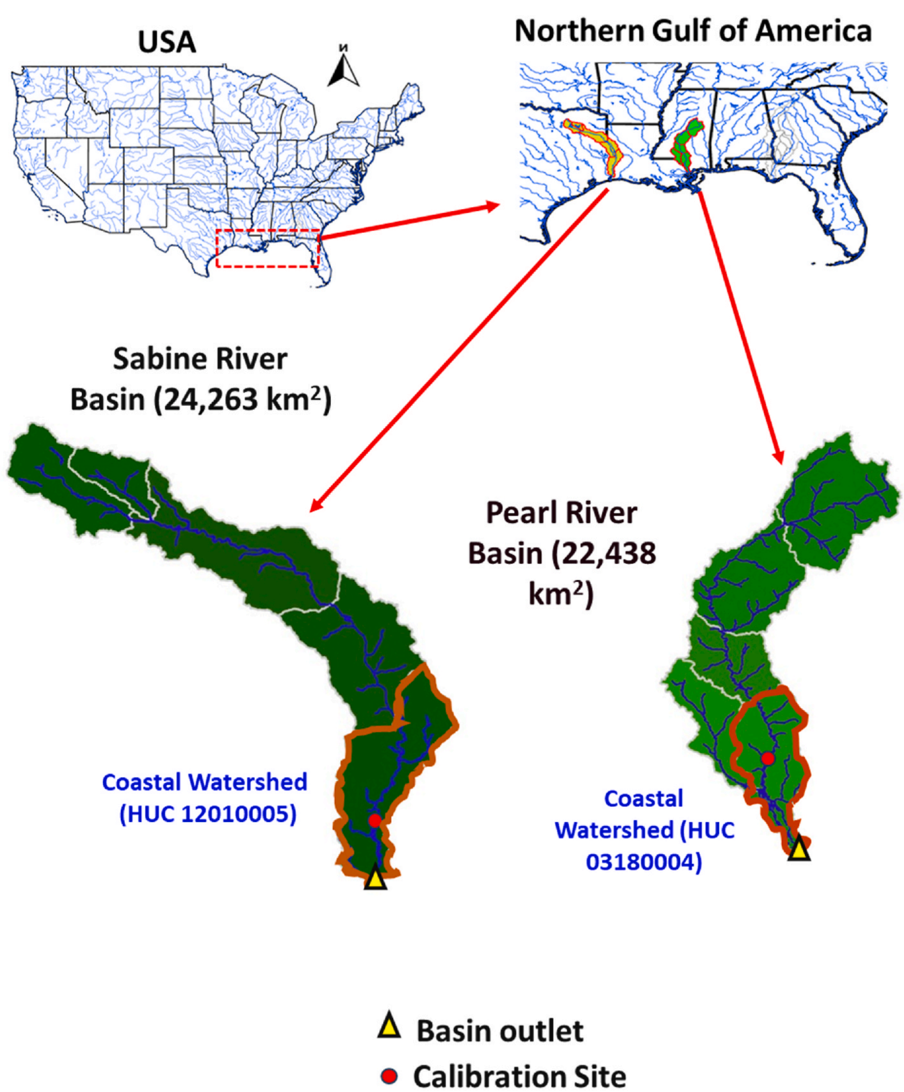

Fig. 1. Location of the Northern Gulf of America, showing the Sabine River Basin and Pearl River Basin and their coastal (outlet) watersheds.

specific objectives are to: (1) develop HAWQS models for the SRB and PRB, with appropriate calibrations and validations; (2) compare the simulated monthly, seasonal, and annual ETs and water yields in the coastal watersheds of these basins between the past and future weather scenarios using the Mann-Kendall (M-K) and Kolmogorov-Smirnov (K-S) tests; and (3) estimate spatial variations of watershed-scale ET and water yield between the past and future scenarios within each basin and across the basins.

2. Materials and methods

2.1. Study basins

The Sabine River Basin (SRB) covers an area of 24,263 km^2, with approximately 76 % in eastern Texas and 24 % in western Louisiana. The basin is about 483 km long and averages 48 km in width, encompassing parts of 20 counties in Texas and six parishes in Louisiana (Hughes and Leifeste, 1965; SRAT-TWDB 1999 Comprehensive Sabine Watershed Management Plan). The Sabine River originates northeast of Dallas, Texas, and flows southeast toward Logansport, Louisiana, eventually widening near its mouth to form Sabine Lake before discharging into the NGOA. The upper SRB, located in the northern region, experiences cool winters, hot summers, and seasonal rainfall patterns, while the lower SRB, in the southern region, has a coastal weather with mild winters, high rainfall, and moderate to high humidity (SRAT-TWDB 1999 Comprehensive Sabine Watershed Management Plan). Annual precipitation in the SRB ranges from 1016 mm in the far north to 1499 mm near the NGOA. The basin includes five watersheds: the Upper Sabine River (HUC-12010001, 3538 km^2), Lake Fork Creek (HUC-12010003, 1755 km^2), Middle Sabine River (HUC-12010002, 7226 km^2), Lower Middle Sabine River (HUC-12010004, 6133 km^2), and Lower Sabine River (HUC-12010005, 6657 km^2). Land use in the SRB is 58 % forest, 34 % pasture and range, 4 % residential, and 4 % other. The soils in the basin belong to three major series: Blackland Prairie, East Texas Timberland, and Coastal Prairie. The Blackland Prairie soils, found in the uppermost part of the SRB, are clayey and prone to erosion. The East Texas Timberland series, which covers nearly 90 % of the SRB, consists of light-colored sandy loam that is also vulnerable to erosion. The Coastal Prairie soils, located near the Gulf Coast, are primarily dark gray to black clays with flat topography, poor drainage, and grassy vegetation, resulting in lower erosion (SRAT-TWDB 1999 Comprehensive Sabine Watershed Management Plan).

The PRB has a drainage area of 22,533 km^2, covering all or parts of 24 counties in Mississippi and three parishes in Louisiana. About one million people live in the basin and more than one-third are residents of Mississippi (MDEQ, 2007). The Pearl River, approximately 790 km long, originates in east-central Mississippi and flows into the NGOA. The PRB consists of five watersheds: Upper Pearl River (HUC-03180001, 6379 km^2), Middle Pearl River (HUC-03180002, 5120 km^2), Lower-Middle Pearl River (HUC-03180003, 3156 km^2), Lower Pearl River (HUC-03180004, 4717 km^2), and Bogue Chitto River (HUC-03180005, 3130 km^2). The average maximum temperature in July is 33.4 °C, and the average minimum temperature in January is 0.3 °C. Annual precipitation averages 1412 mm, with a wet period from November to April and a dry period from May to October. Land cover is dominated by 69 % forest, 27 % agricultural land, and 3 % wetland and waterbodies (Ouyang et al., 2023). Predominant soil types are fine sandy loam and silt loam (Parajuli, 2010). The basin contains over 14,000 ha of intact bottomland hardwood forest, including mixed hardwoods such as various oaks (Quercus spp.), sweetgum (Liquidambar styraciflua), hickories (Carya spp.), and elms (Ulmus spp.) (Chapman et al., 2008).

2.2. Basin model development and data acquisition

HAWQS is a web-based interactive system for simulating water quantity and quality in watersheds across the lower 48 U.S. states (https://hawqs.tamu.edu/#/). It uses the Soil and Water Assessment Tool (SWAT) model (Arnold et al., 2012) as its core engine and provides users with interactive maps, pre-loaded data, and simulation outputs like tables and charts. More specifically, HAWQS is a customized version of SWAT to simulate impacts of crop, soil, natural vegetation types, land uses, and others agricultural management practices on watershed hydrological processes (*e.g.*, evapotranspiration, surface runoff, streamflow, and water yield) and water quality constituents (*e.g.*, sediment, pathogens, nutrients, biological oxygen demand, dissolved oxygen, pesticides, and water temperature) under a changing weather. The United States Environmental Protection Agency (EPA) provides funding for HAWQS development and the Texas A&M University and EPA subject matter experts provide ongoing technical support. The elaborate descriptions of HAWQS can be found at https://hawqs.tamu.edu/#/, whereas the methods on how to calculate hydrological processes and water quality are documented in the SWAT model users' manual (https://swat.tamu.edu/media/1294/swatuserman.pdf). Many studies have used HAWQS, including Chen et al. (2020), who analyzed evapotranspiration (ET) methods for the Upper Mississippi River Basin and found the PRISM (Parameter-elevation Regressions on Independent Slopes Model) weather dataset to be the most reliable. Ouyang et al. (2023) used HAWQS to project sediment load reductions in the Lower Mississippi Basin under future weather scenarios with afforestation, reporting a 10 % reduction by 2064.

In this study, the basin-scale models were developed for the SRB and PRB using HAWQS. The main steps included: (1) Create a project. Select the watersheds that have the basin outlets at a watershed resolution of HUC8 and set the HRU (Hydrologic Response Units) to 1 %. The watersheds that cover the basin outlets include HUC8-12010005 for the SRB and HUC8-03180004 for the PRB (Fig. 1). A 1 % threshold of HRUs was used to remove the land use areas that are <1 %; (2) Set up scenarios and customize input data. Two simulation scenarios (*i.e.*, the past and future scenarios) were used in this study. The past scenario investigated the ET and water yield from 1985 to 2024 (40 years), whereas the future scenario estimated the same hydrological processes from 2025 to 2064 (40 years). The past weather dataset was from PRISM, while the future weather dataset was from the CCSM4 (Community Weather System Model 4) with the RCP85 (Representative Concentration Pathway 85). It should be noted that a 40-year simulation period is used for both scenarios because the past weather dataset from PRISM in HAWQS is only available from 1981 to 2024. Excluding the model warm-up years, the 40-year simulation period is suitable for this study; (3) Run the simulation scenarios; and (4) Analyze the simulation outputs. Details on how to develop and run the HAQWS model can be found at https://hawqs.tamu.edu/#/.

All the past and future weather scenario datasets are readily available in HAWQS. For the past scenarios, there are two actual weather datasets, namely the PRISM and NEXRAD (Next Generation Weather Radar), have been pre-loaded into the HAWQS model for all watersheds and/or basins across the continental U.S. For the future weather scenarios, the CMIP5 (Coupled Model Intercomparison Project Phase 5) dataset has been pre-load into the HAWQS model for all watersheds and/or basins across the continental U.S. The CMIP5 includes 12 future weather sub-scenarios such as CanESM2 (Second Generation Canadian Earth System Model), CCSM4, and MIROC5 (Model for Interdisciplinary Research on Weather version 5). Users can just simply choose the weather scenarios and the associated dataset they prefer from the Weather Data Section of the HAWQS model. Similarly, all basin and/or watershed characteristics, soil types, land uses, vegetation covers, and other data necessitate for running the HAWQS model across the continental U.S. have been pre-loaded into the HAWQS model as well. When users select a watershed or basin of interested, all these data are automatically loaded into the HAWQS model.

2.3. Statistical analysis and model calibration and validation

Trends in ET, water yield, and precipitation were analyzed using the Mann-Kendall test, a nonparametric test suited for time series analysis. The τ value (ranging from −1 to 1) indicates the strength of the trend, with $\tau = 0$ meaning no trend, and $\tau = 1$ or -1 showing a perfect trend (positive for increasing, negative for decreasing). A p-value ≤ 0.05 indicates a significant trend. The analysis was performed in R. An elaborate description of Mann-Kendall theory is reported in Kendall et al. (1994).

Differences between past and future hydrological processes (ET, water yield, and precipitation) were evaluated using the Kolmogorov-Smirnov (K-S) test. This test compares two sample distributions, and the samples are statistically different if the K-S D statistic is less than the critical value at $\alpha = 0.05$. The K-S test was conducted using a web-based tool (https://www.aatbio.com/tools/kolmogorov-smirnov-k-s-test-calculator). Details on the K-S statistics are given in Solari (1967).

Model calibration is a process to match model predictions with field observations by adjusting values of model input parameters. In this study, the goodness-of-fit of model calibration was assessed using the Nash-Sutcliffe efficiency (NSE), percent bias (PBIAS), and Kling-Gupta efficiency (KGE) methods (Knoben et al., 2019; Moriasi et al., 2015; Rubin, 1976). Calculations were accomplished in Excel except for KGE that was calculated with Python script. The SRB and PRB models were calibrated using discharge data from US Geological Survey (USGS). Input parameters related to water balance, surface runoff, and reach parameters were adjusted to align predicted discharge with observed data. Table 1 lists key parameter values and statistics (*i.e.*, NSE, PBIAS, and KGE) from the calibration, along with the USGS monitoring stations and calibration periods. Based on these metrics, the models performed well in predicting discharge during model calibration.

Model validation is a process to verify model predictions with another dataset of field observations (i.e., different from the dataset used for model calibration) without changing any values of input parameters. Table 1 provides the data sources and periods used during model validation. The goodness-of-fit of model validation was also estimated using the NSE, PBIAS, and KGE methods. Based on the good statistical metrics (Table 1) and reasonable matches between predicted and observed discharges (Fig. S1), the models were well verified during model validation.

3. Results and discussion

3.1. Monthly variations

Figures 2–3 (left panels) compare monthly ET, water yield, precipitation, and air temperature in coastal watersheds between past and future scenarios. In this study, monthly ET and water yield were model outputs, whereas monthly precipitation and air temperature were model inputs. The coastal watersheds here refer to those adjacent to coastal areas and include the basin outlets, with HUC numbers 12010005 for the SRB and 03180004 for the PRB (Fig. 1). In general, monthly ET in the two coastal watersheds increased from January to May (or June) and then decreased to December for both past and future scenarios (Figs. 2a and 3a). The highest ET occurred in May (or June) and the lowest in January for both scenarios. This pattern was driven by the corresponding high air temperature in May (or June) and low air temperature in January (Figs. 2d and 3d), highlighting the significant role air temperature played in monthly ET. This typical monthly ET pattern was consistent with findings reported in the literature (Feng et al., 2016; Hillel, 2003; Shukla, 2023). Feng et al. (2016) investigated reference ET over 120 years (1894–2014) in the Blackland Prairie, Mississippi, which locates above the north of the PRB. These authors reported that monthly ET ranged from 38 to 158 mm with an average of 97 mm over 120 years. The current study showed that monthly ET ranged from 30 to 116 mm with an average of 70 mm for the past scenario and 46–141 mm with an

Table 1
Major input parameter values used for calibrations and validations of the Sabine River basin (SRB) and Pearl River Basin (PRB) models. The statistical measures for goodness-of-fit are also provided.

Input Variable	Definition/Unit	Value for SRB	Value for PRB
Water Balance			
SFTMP	Snowfall temperature (°C)	0.138	−0.8668
SMTMP	Snow melt base temperature (°C)	0.994	0.2662
SMFMX	Maximum melt rate for snow during the year (occurs on summer solstice) (mm/°C-day)	4.52	4.33
SMFMN	Minimum melt rate for snow during the year (occurs on summer solstice) (mm/°C-day)	3.114	3.165
TIMP	Snow pack temperature lag factor	0.313	0.08844
IPET	Potential evapotranspiration method	2	2
ESCO	Soil evaporation compensation factor	0.95	0.95
EPCO	Plant uptake compensation factor	1	1
Surface Runoff			
ICN	Daily curve number method	0	0
CNCOEF	Plant ET curve number coefficient	1	1
ICRK	Crack flow code	0	0
SURLAG	Surface runoff lag time	21.34	1.079
Reach			
IRTE	Channel water routing method	0	0
MSK_COL1	Calibration coefficient used to control impact of the storage time constant for normal flow	0	0
MSK_COL2	Calibration coefficient used to control impact of the storage time constant for low flow	3.5	3.5
MSK_X	Weighting factor controlling relative importance of inflow rate and outflow rate in determining water storage in reach segment	0.2	0.2
TRNSRCH	Fraction of transmission losses from main channel that enter deep aquifer	0	0
EVRCH	Reach evaporation adjustment factor	1	1
IDEG	Channel degradation code	0	0
PRF	Peak rate adjustment factor for sediment routing in the main channel	1	1
SPCON	Linear parameter for calculating the maximum amount of sediment that can be reentrained during channel sediment routing	0	1
SPEXP	Exponent parameter for calculating sediment reentrained in channel sediment routing	1	1
IWQ	In-stream water quality code	1	1
ADJ_PKR	Peak rate adjustment factor for sediment routing in the subbasin (tributary channels)	0.5	0.5
Model Calibration			
NSE	Nash-Sutcliffe efficiency	0.59	0.69
PBIAS	Percent Bias	−13.8	18.61
KGE	Kling-Gupta efficiency	0.67	0.72
USGS Station #	US Geological Survey stream flow monitoring stations used for model calibration	08030500	02359170
Calibration Period	Time period of the observed data used for model calibration	2000–2010	1998–2008
Model Validation			
NSE	Nash-Sutcliffe efficiency	0.54	0.5
PBIAS	Percent Bias	−4.1	19.38
KGE	Kling-Gupta efficiency	0.86	0.69
USGS Station #	US Geological Survey stream flow monitoring stations used for model validation	08030500	02359170
Validation Period	Time period of the observed data used for model validation	2010–2015	2008–2018

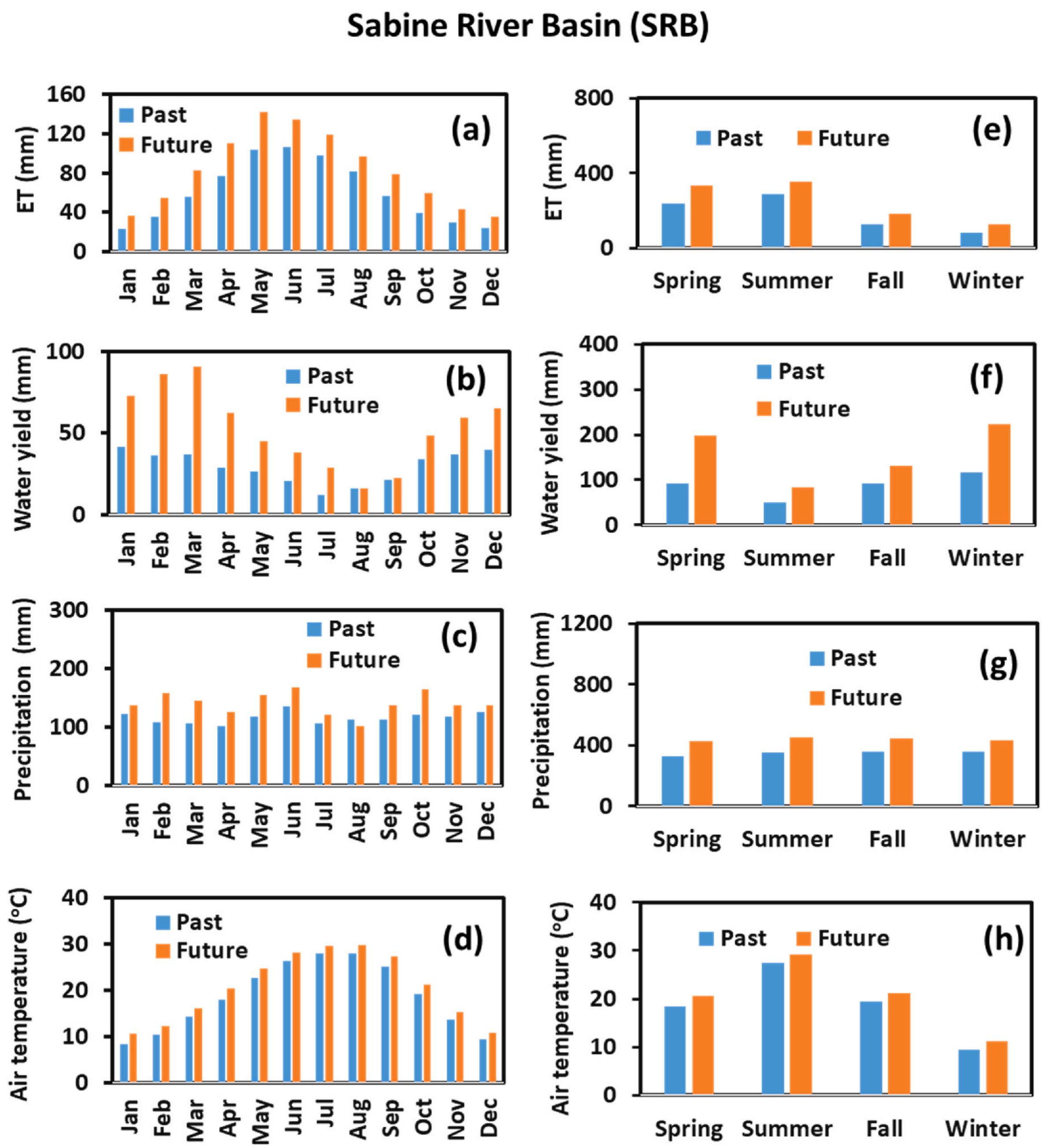

Fig. 2. Monthly (left panel) and seasonal (right panel) ET, water yield, precipitation, and air temperature between past and future scenarios at the coastal watershed of the Sabine River Basin.

average of 94 mm for the future scenario at the PRB. These findings were consistent and within the span to those reported by Feng et al. (2016). Results indicated that longitudinal variation of monthly ET from the coastal area to the northern part of Mississippi was small.

Figs. 2a and 3a further reveal that while monthly ET for the future scenario was slightly higher than those for the past scenario, the differences were statistically insignificant based on the K-S test (Table S1), indicating that weather variation had a minimal effect on ET over the 80-year period.

Unlike the case of monthly ET, mixed results were found for monthly water yield. In the past scenario, water yield decreased from January to July and increased from August to December in the coastal watersheds of the SRB and PRB (Figs. 2b and 3b). In the future scenario, water yield increased from January to March, decreased from March to August, and increased again from August to December. These changes could be linked to variations in precipitation between the scenarios. In the past scenario, precipitation decreased from January to May (Figs. 2c and 3c), leading to water yield reduction. In the future scenario, however, precipitation increased significantly from January to March, resulting in higher water yield during this period. These findings align with earlier research by Pessacg et al. (2015) and Wu et al. (2022). Pessacg et al. (2015) estimated water yield in the Chubut River basin, Argentina using six widely used global precipitation datasets and reported that water yield was highly sensitive to precipitation. Wu et al. (2022) investigated water yield in response to precipitation in the Weihe River Basin, China and concluded that precipitation was the main factor affecting water yield in the basin.

In the past scenario, maximum water yield occurred in January for the coastal watersheds of the SRB (41 mm, Fig. 2b) and PRB (63 mm, Fig. 3b). Maximum water yield typically coincides with high

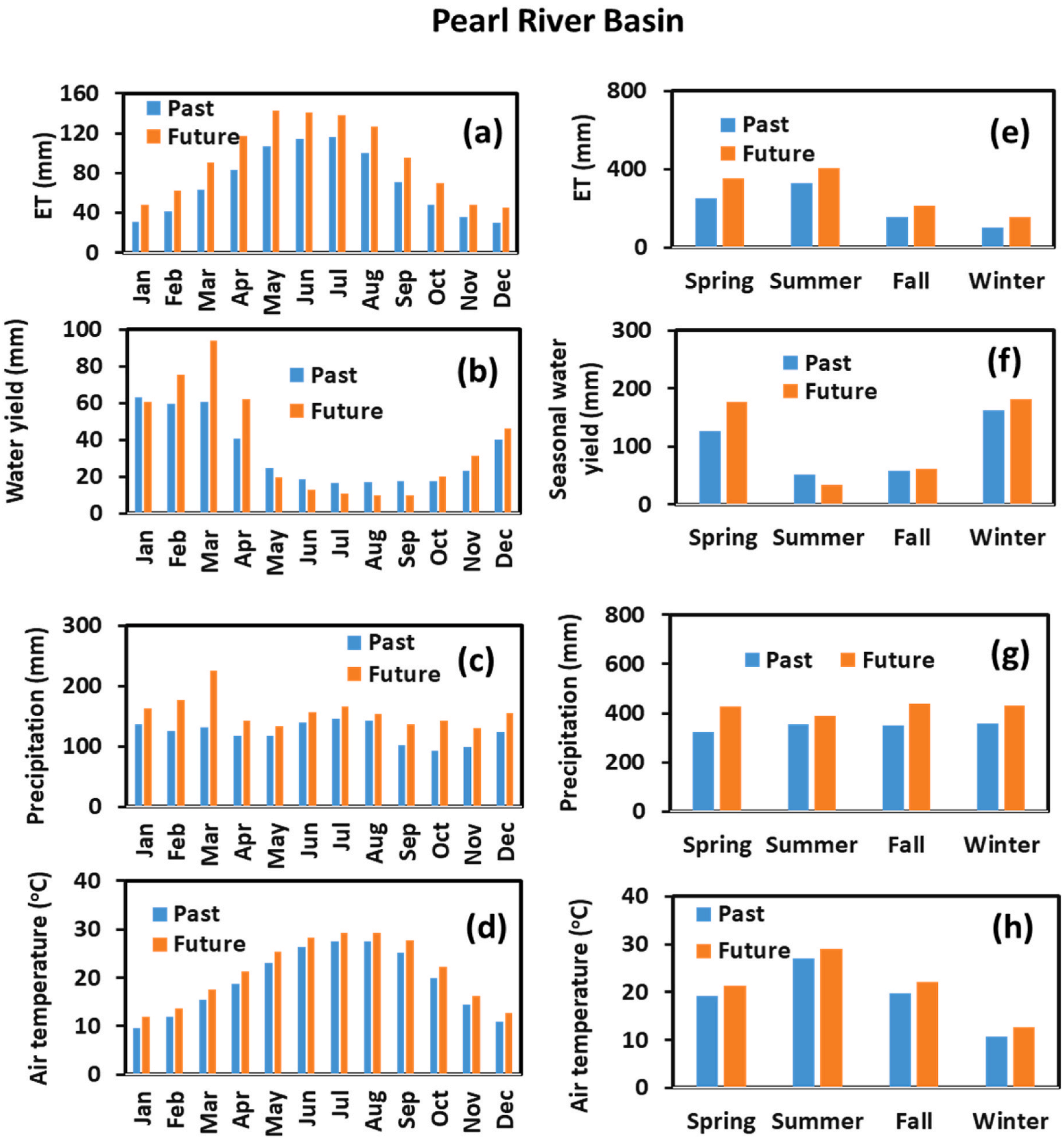

Fig. 3. Monthly (left panel) and seasonal (right panel) ET, water yield, precipitation, and air temperature between past and future scenarios at the coastal watershed of the Pearl River Basin.

precipitation and low air temperature, which reduces ET and allows more water to contribute to water yield. In the future scenario, maximum water yield shifted to March for the coastal watersheds of the SRB (90 mm) and PRB (94 mm). These peaks were closely aligned with maximum monthly precipitation. A notable finding was the two-month shift in maximum monthly water yield from January to March in the coastal watersheds of the SRB and PRB, which highlights the influence of weather variation — specifically increased precipitation in the future scenario. Results demonstrated that the month with maximum water yield occurred under a changing weather in the coastal watersheds of the NGOA depended on monthly precipitation. Very few efforts have been devoted to estimating water yield in the coastal watersheds of the PRB and SRB. This study provided critical reference to water resource managers on how weather variation shifting monthly maximum water yield in the regions and could provide hints to other regions around the world.

3.2. Seasonal variations

In this study, seasons were defined as spring (March–May), summer (June–August), fall (September–November), and winter (December–February). Seasonal variations in ET, water yield, precipitation, and air temperature at the coastal watersheds (Figures 2–3, right panels) followed expected patterns for both past and future scenarios. Seasonal ET increased from spring to summer and decreased from summer to winter, with the highest values in summer and the lowest in winter. The order of seasonal ET was summer > spring > fall > winter for both scenarios (Figs. 2e and 3e), closely following seasonal air temperature (Figs. 2h and 3h) as warmer temperature promoted higher ET. Compared to the past scenario, the seasonal ET in the future scenario in summer at the coastal watersheds increased by 18.5 % for the SRB and 18.4 % for the PRB. A similar increasing ET trend was also noted by Neupane et al. (2019). These authors applied the SWAT model to estimate the potential hydrologic changes for the mid-21st century (2050s) and the late 21st century (2080s) in the Mobile River, Apalachicola River, and Suwannee River watersheds in the Gulf Coast region and projected about 10 % increase in seasonal ET in the Apalachicola River watershed by 2050 as air temperature increased. However, the statistical test on the seasonal ET difference between past and future scenarios was not performed by Neupane et al. (2019). In the current study, the seasonal differences of ET at the coastal watersheds between past and future scenarios were found to be statistically insignificant (K-S test, Table S1). Results implied that weather variation had minor impact on seasonal ET over the 80-year period.

Figs. 2 and 3 further revealed that seasonal ET was consistently higher in spring and summer than in fall and winter for both past and future scenarios. For example, at the PRB's coastal watershed, spring and summer averaged 292 mm of ET in the past scenario and 378 mm in the future, compared to 128 mm and 185 mm in fall and winter, respectively. In other words, the seasonal ET was 2.1 times higher during spring and summer (292 + 378 = 670 mm) than during fall and winter (128 + 185 = 313 mm). This information can help water resource managers mitigate seasonal water evaporative loss in coastal watersheds of the NGOA.

Seasonal water yield followed the order: winter > spring > fall > summer (Figs. 2f and 3f), with maximum water yield in winter and minimum in summer. This reflected the inverse relationship between ET and water yield. That is, higher ET in summer resulted in lower water yield, while lower ET in winter led to higher water yield. Seasonal precipitation also influenced water yield, but as seen in the SRB and PRB, its impact was not the sole factor, with large variations in water yield despite small seasonal differences in precipitation (Figs. 2g and 3g). This suggests that seasonal ET also played a crucial role in governing seasonal water yield. Analogous to the case of seasonal ET, the seasonal differences in water yield at the coastal watersheds between past and future scenarios were statistically insignificant based on the K-S test (Table S1), indicating weather variation on seasonal water yield was minimal.

Unlike the case of seasonal ET, seasonal water yield was higher during spring and winter than during summer and fall for both past and future scenarios. For instance, at the SRB's coastal watershed, the seasonal water yield during spring and winter was 422 mm and during summer and fall was 213 mm in the future scenario. The sum of former two-season water yield was 1.98 times higher than the latter two-season water yield. Very little effort has been devoted to estimating seasonal variation of water yield in the SRB, PRB, and NGOA. This study fills the information gap in the region.

3.3. Annual variation

Annual average ET, water yield, and precipitation for the coastal watersheds of the SRB and PRB were slightly or moderately higher in the

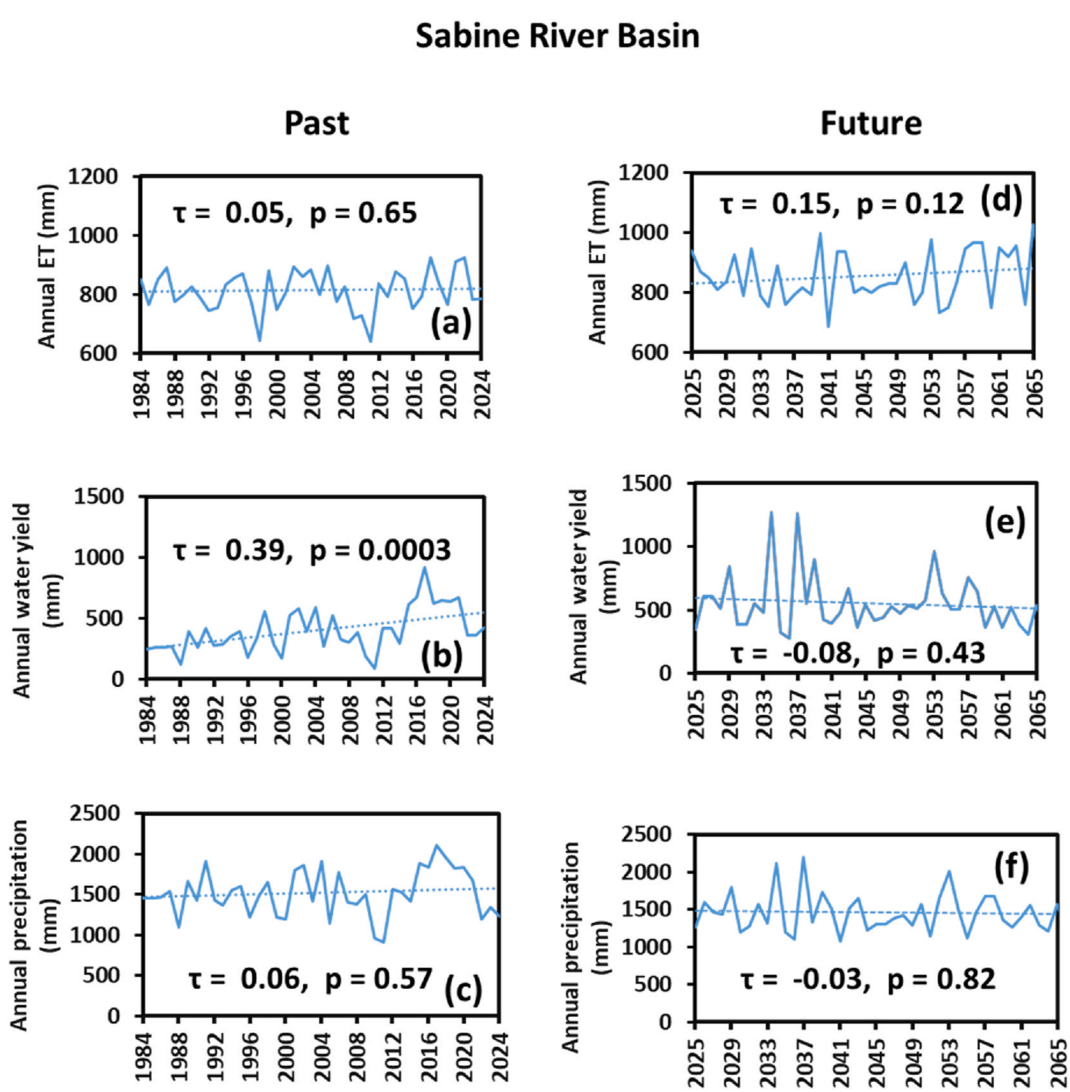

Fig. 4. Annual trends of ET, water yield, and precipitation at the coastal watershed of the Sabine River Basin between past and future scenarios.

future scenario than in the past (Fig. S2). However, only the SRB's coastal watershed showed statistically significant differences in annual ET and water yield between the two scenarios (K-S test, Table S1), indicating that the effects of weather variation on these parameters varied with coastal watersheds. It is also worthy of mentioning here that some studies in the literature have not performed statistical tests when comparing the differences of hydrological processes, resulting from the past and future weathers. This kind of analyses may not be appropriate.

Annual time series trends for ET, water yield, and precipitation in the past scenario (Figures 4–5, left panels) revealed no significant trends for precipitation in any basin. For the future scenario, no significant trends were observed (Figures 4–5, right panels), suggesting that weather variation impacts on annual trends may be less pronounced moving forward in the coastal watersheds of the NGOA. Little effort has been devoted to predicting future trends of ET and water yield in the coastal watersheds of the NGOA. Using the DLEM model, Liu et al. (2013) estimated the temporal trend of ET in the GOM during 1901–2008 and reported a significant decreasing trend of ET during this period. Their finding was inconsistent with results from this study. As shown in Fig. 4a-5a (left, panels), the annual ET had no or increasing trend in the past scenario. This discrepancy occurred because Liu et al. (2013) used all watersheds of the GOM as their modeled domain, while this study focused on coastal watersheds of the NGOA.

3.4. Spatial variability

Spatial variability of annual average ET, water yield, and precipitation in each watershed of the two basins in the past (left panel) and future (right panel) scenarios is shown in Figures 6–7. The numbers in the parentheses of the figures are the average values, whereas the numbers marked in the watersheds of the figures are the watershed numbers. In both scenarios, annual ET was lower in northernmost (inland) watersheds and higher in southernmost (coastal) watersheds across all basins. For instance, in the SRB, ET was 644 mm in the northernmost watershed (#1) and 809 mm in the southernmost watershed (#5) for the past scenario (Fig. 6a). This pattern was driven by higher precipitation in the southernmost watersheds (Fig. 6c), providing more water for ET. For the past scenario, the average annual ETs in the northernmost (inland) watersheds were 25 % ([809–644]/644) and 5 % ([929-885]/885) lower than those in southernmost (coastal) watersheds, respectively, for the SRB and PRB. For the future scenario, the average annual ETs in the northernmost (inland) watersheds were 28 % ([860–671]/671) and 2 % ([973-956]/956) lower than those in southernmost (coastal) watersheds, respectively, for the SRB and PRB. Apparently, spatial variability of annual average ET was larger in the SRB than in the PRB.

A comparison of past and future scenarios showed higher ET in future scenarios across all watersheds. For example, ET in Watershed #3 of the PRB increased from 947 mm in the past to 1012 mm in the future, a 7 % increase, driven by higher air temperatures and precipitation (Figs. 3d and 7c). However, these differences were statistically insignificant based on the K-S test (Table S1), suggesting that weather variation had a limited effect on annual average ET at the two basins.

Annual average water yield also varied across watersheds within a

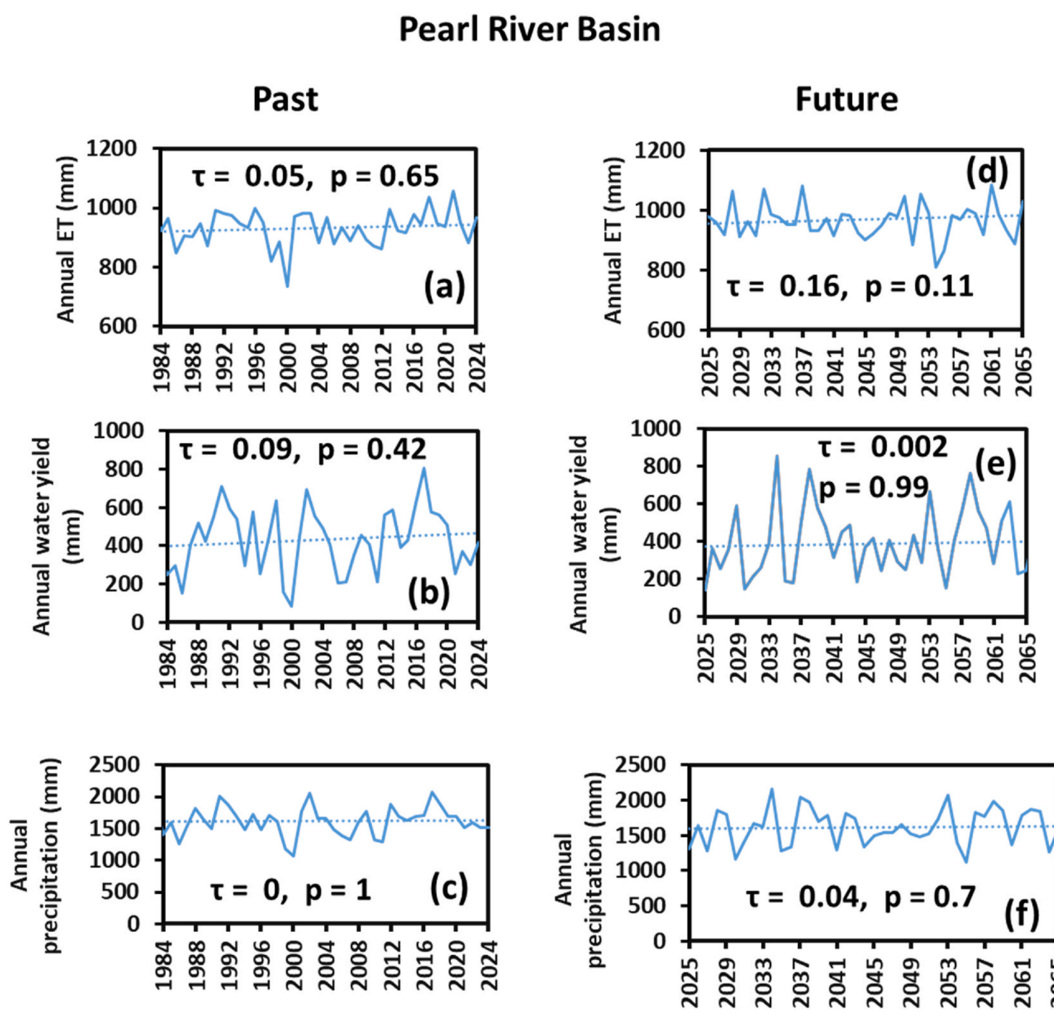

Fig. 5. Annual trends of ET, water yield, and precipitation at the coastal watershed of the Pearl River Basin between past and future scenarios.

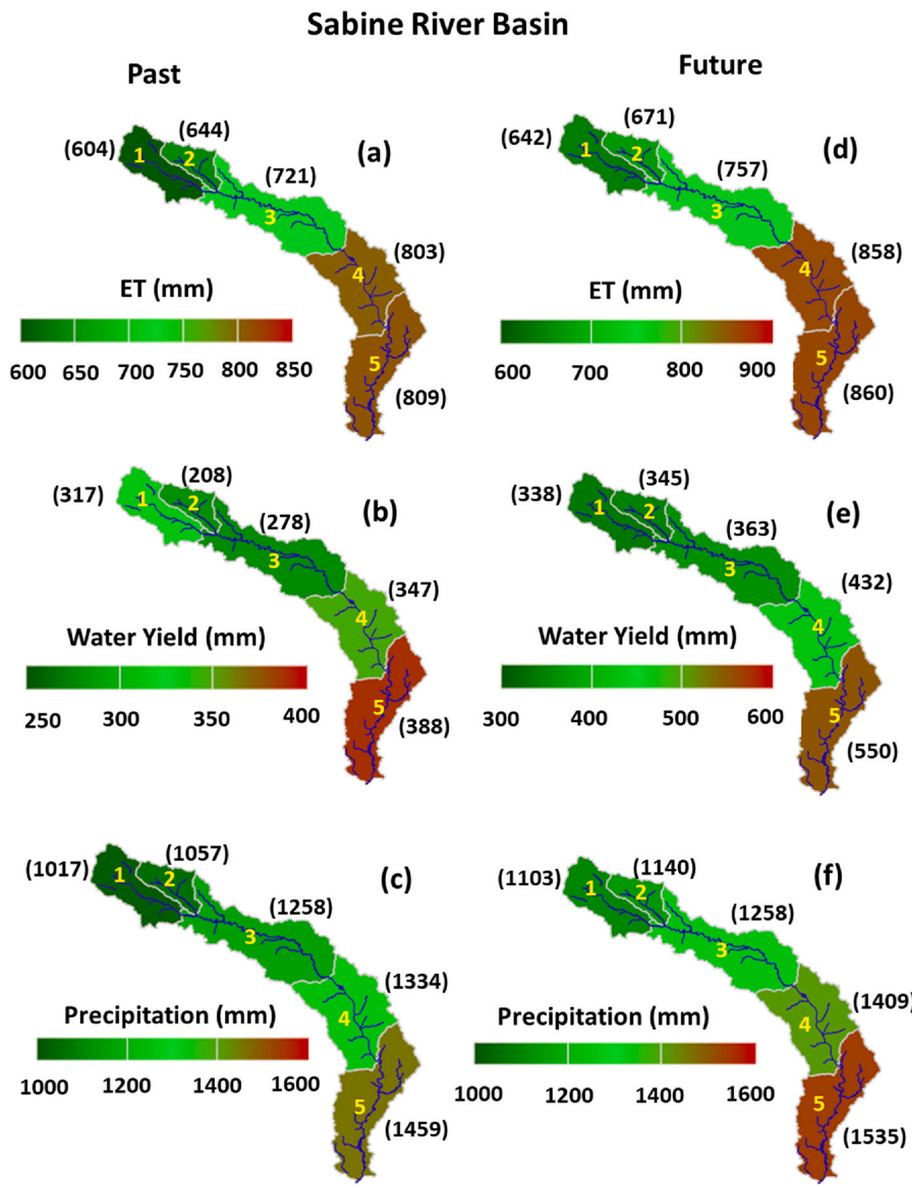

Fig. 6. Spatial distributions of annual ET, water yield, and precipitation among watersheds at the Sabine River Basin.

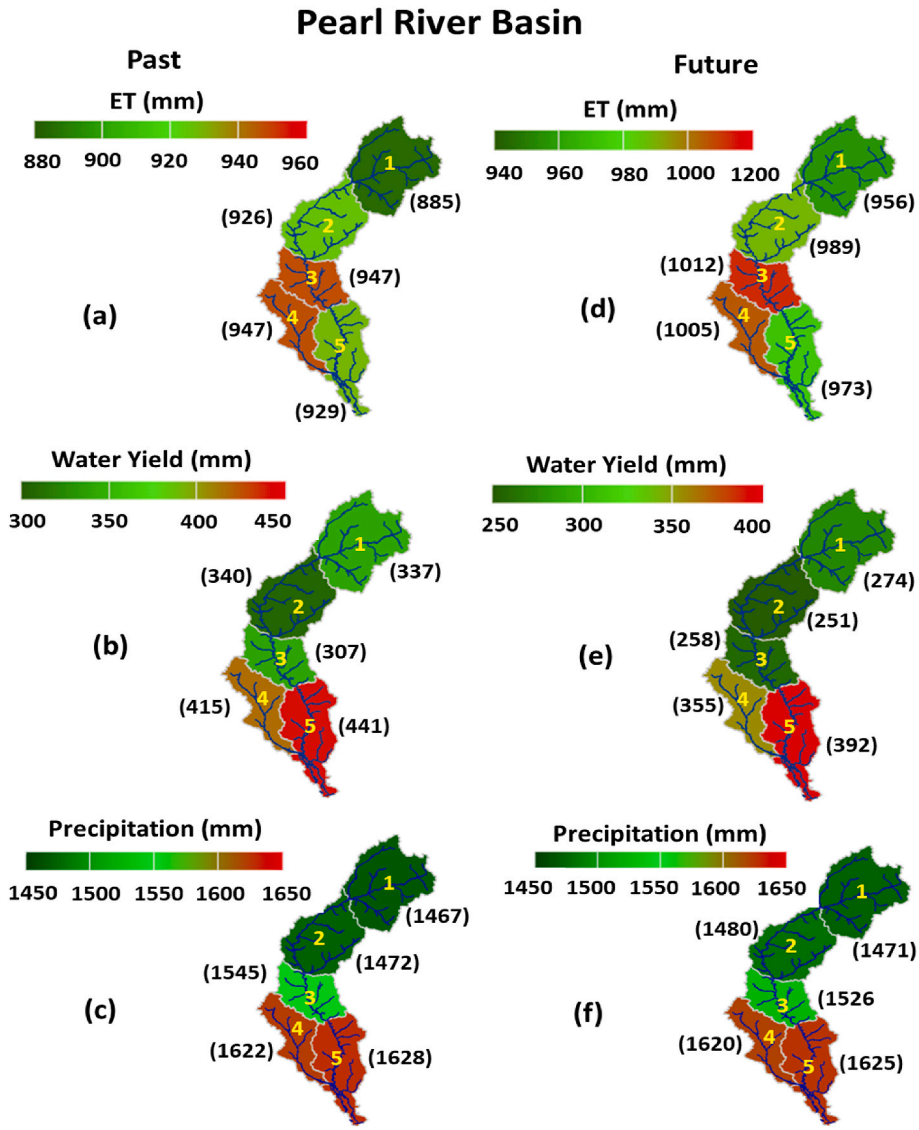

Fig. 7. Spatial distributions of annual ET, water yield, and precipitation among watersheds in the Pearl River Basin.

basin. In the past scenario, the highest annual water yield was found in the southernmost watersheds of two basins with 388 mm for the SRB (Fig. 6b) and 441 mm for the PRB (Fig. 7b). In the future scenario, the highest annual water yield was observed at the southernmost watersheds with 550 mm for the SRB (Fig. 6e) and 392 mm for the PRB (Fig. 7e). A closer look at the annual water yield and precipitation revealed that this highest annual water yield was linked to the highest precipitation. Results showed that precipitation, along with lower ET and other factors, played a key role in determining annual water yield.

4. Conclusions

While monthly ET in the future scenario was higher than in the past scenario, the difference was not statistically significant. Therefore, impacts of weather variation on monthly ET over the 80-year period in the coastal watersheds of the NGOA were minimal. A two-month shift in the timing of maximum monthly water yield, moving from January in the past scenario to March in the future scenario was found at the coastal watersheds.

Seasonal ET was roughly twice as high in spring and summer compared to fall and winter, while seasonal water yield was about twice as large in spring and winter compared to fall and summer. An increase in summer precipitation did not result in a higher summer water yield as seasonal ET also influencing seasonal water yield.

Annual water yield varied from watershed to watershed within each basin, with precipitation being the key factor. However, ET and other watershed conditions also played significant roles in determining water yield. Annual average ET was lower in the northernmost (inland) watersheds than in the southernmost (coastal) watersheds for the two basins in both past and future scenarios.

Declaration of competing interest

The authors declare that they have no known competing financial interests or personal relationships that could have appeared to influence the work reported in this paper.

Appendix A. Supplementary data

Supplementary data to this article can be found online at https://doi.org/10.1016/j.jenvman.2025.125157.

Data availability

Data will be made available on request.

References

Allen, R.G., Jensen, M.E., Wright, J.L., Burman, R.D., 1989. Operational estimates of reference evapotranspiration. Agron. J. 81 (4), 650–662.

Arnold, J.G., Moriasi, D.N., Gassman, P.W., Abbaspour, K.C., White, M.J., Srinivasan, R., Santhi, C., Harmel, R.D., van Griensven, A., Van Liew, M.W., Kannan, N., Jha, M.K., 2012. Swat: model use, calibration, and validation. T Asabe 55 (4), 1491–1508.

Cemek, B., Tasan, S., Canturk, A., Tasan, M., Simsek, H., 2023. Machine learning techniques in estimation of eggplant crop evapotranspiration. Appl. Water Sci. 13 (6).

Chapman, E.L., Chambers, J.Q., Ribbeck, K.F., Baker, D.B., Tobler, M.A., Zeng, H.C., White, D.A., 2008. Hurricane Katrina impacts on forest trees of Louisiana's Pearl River basin. For. Ecol. Manag. 256 (5), 883–889.

Chen, M., Gassman, P.W., Srinivasan, R., Cui, Y., Arritt, R., 2020. Analysis of alternative weather datasets and evapotranspiration methods for the Upper Mississippi River Basin using SWAT within HAWQS. Sci. Total Environ. 720, 137562.

Feng, G., Cobb, S., Abdo, Z., Fisher, D.K., Ouyang, Y., Adeli, A., Jenkins, J.N., 2016. Trend analysis and forecast of precipitation, reference evapotranspiration, and rainfall deficit in the Blackland Prairie of Eastern Mississippi. J. Appl. Meteorol. Climatol. 55 (7), 1425–1439.

Fisher, D.K., Pringle III, H., 2013. Evaluation of alternative methods for estimating reference evapotranspiration. Agric. Sci. 2013.

Gizaw, M.S., Biftu, G.F., Gan, T.Y., Moges, S.A., Koivusalo, H., 2017. Potential impact of weather variation on streamflow of major Ethiopian rivers. Clim. Change 143 (3–4), 371–383.

Hillel, D., 2003. Introduction to Environmental Soil Physics. Elsevier.

Hughes, L.S., Leifeste, D.K., 1965. Reconnaissance of the Chemical Quality of Surface Waters of the Sabine River Basin, Texas and Louisiana. US Government Printing Office.

Jones, J.A., Perkins, R.M., 2010. Extreme flood sensitivity to snow and forest harvest, western Cascades, Oregon, United States. Water Resour. Res. 46.

Judd, L.J., 1995. Gulf of Mexico program (U.S.) and geological Survey (U.S.). Streamflow to the Gulf of Mexico. U.S. Dept. of the Interior Earth Science Information Center, Open-File Reports Section [distributor], Austin, Tex. Denver, CO.

Keller, A.A., Garner, K., Rao, N., Knipping, E., Thomas, J., 2023. Hydrological models for weather-based assessments at the watershed scale: a critical review of existing hydrologic and water quality models. Sci. Total Environ. 867.

Kendall, M.G., Stuart, A., Ord, J.K., Arnold, S.F., O'Hagan, A., 1994. Kendall's Advanced Theory of Statistics, Edward Arnold. Halsted Press, London; New York.

Knoben, W.J., Freer, J.E., Woods, R.A., 2019. Inherent benchmark or not? Comparing nash–sutcliffe and kling–gupta efficiency scores. Hydrol. Earth Syst. Sci. 23 (10), 4323–4331.

Liu, M.L., Tian, H.Q., Yang, Q.C., Yang, J., Song, X., Lohrenz, S.E., Cai, W.J., 2013. Long-term trends in evapotranspiration and runoff over the drainage basins of the Gulf of Mexico during 19012008. Water Resour. Res. 49 (4), 1988–2012.

MacDonald, P.O., Frayer, W.E., Clauser, J.K., Forsythe, S.W., U.S. Fish and Wildlife Service. Division of Ecological Services. and HRB-Singer Inc, 1979. Documentation, Chronology, and Future Projections of Bottomland Hardwood Habitat Loss in the Lower Mississippi Alluvial Plain. Ecological Services, Fish and Wildlife Service, U.S. Dept. of the Interior, [Washington, D.C.].

McKee, P.W., Clark, B.R., Czarnecki, J.B., United States. Army. Corps of Engineers. Memphis District., Arkansas Soil and Water Conservation Commission. and Geological Survey (U.S.), 2004. Conjunctive-use Optimization Model and Sustainable-Yield Estimation for the Sparta Aquifer of Southeastern Arkansas and North-Central Louisiana. U.S. Dept. of the Interior Branch of Information Services [distributor], Little Rock, Ark. Denver, Colo.

McKinney, L.D., Shepherd, J.G., Wilson, C.A., Hogarth, W.T., Chanton, J., Murawski, S. A., Sandifer, P.A., Sutton, T., Yoskowitz, D., Wowk, K., 2021. The gulf of Mexico. Oceanography (Wash., D.C.) 34 (1), 30–43.

MDEQ 2007 Citizen's Guide to Water Quality in the Pearl River Basin.

Mokhtari, A., Sadeghi, M., Afrasiabian, Y., Yu, K., 2023. OPTRAM-ET: a novel approach to remote sensing of actual evapotranspiration applied to Sentinel-2 and Landsat-8 observations. Remote Sens. Environ. 286.

Monteith, J.L., 1965. Evaporation and Environment. The Stage and Movement of Water in Living Organisms. Cambridge University Press.

Moriasi, D.N., Gitau, M.W., Pai, N., Daggupati, P., 2015. Hydrologic and water quality models: performance measures and evaluation criteria. T Asabe 58 (6), 1763–1785.

Neupane, R.P., Ficklin, D.L., Knouft, J.H., Ehsani, N., Cibin, R., 2019. Hydrologic responses to projected weather variation in ecologically diverse watersheds of the Gulf Coast, United States. Int. J. Climatol. 39 (4), 2227–2243.

Oren, R., Ewers, B.E., Todd, P., Phillips, N., Katul, G., 1998. Water balance delineates the soil layer in which moisture affects canopy conductance. Ecol. Appl. 8 (4), 990–1002.

Ouyang, Y., 2021. New insights on evapotranspiration and water yield in crop and forest lands under changing weather. J. Hydrol. 603.

Ouyang, Y., Huang, Y.B., Parajuli, P.B., Wan, Y.S., Grace, J.M., Caldwell, P.V., Trettin, C., 2023. Projection of sediment loading from Pearl River Basin, Mississippi into gulf of Mexico under a future weather with afforestation. Weather 11 (5).

Ouyang, Y., Yang, J., Huang, Y., Leininger, T.D., Chastain, D., 2024. Evidence of higher evapotranspiration in croplands than in forestlands in four Mississippi watersheds over the past decade. Agric. Water Manag. 302, 108992.

Parajuli, P.B., 2010. Assessing sensitivity of hydrologic responses to weather variation from forested watershed in Mississippi. Hydrol. Process. 24 (26), 3785–3797.

Pessacg, N., Flaherty, S., Brandizi, L., Solman, S., Pascual, M., 2015. Getting water right: a case study in water yield modelling based on precipitation data. Sci. Total Environ. 537, 225–234.

Rabalais, N.N., Turner, R.E., Sen Gupta, B.K., Boesch, D.F., Chapman, P., Murrell, M.C., 2007. Hypoxia in the northern Gulf of Mexico: does the science support the plan to reduce, mitigate, and control hypoxia? Estuaries Coasts 30 (5), 753–772.

Rubin, D.B., 1976. Multivariate matching methods that are equal percent bias reducing, I: some examples. Biometrics 109–120.

Scanlon, B.R., Fakhreddine, S., Rateb, A., de Graaf, I., Famiglietti, J., Gleeson, T., Grafton, R.Q., Jobbagy, E., Kebede, S., Kolusu, S.R., Konikow, L.F., Long, D., Mekonnen, M., Schmied, H.M., Mukherjee, A., MacDonald, A., Reedy, R.C., Shamsudduha, M., Simmons, C.T., Sun, A.L., Taylor, R.G., Villholth, K.G., Vörösmarty, C.J., Zheng, C.M., 2023. Global water resources and the role of groundwater in a resilient water future (Jan 2023. Nat. Rev. Earth Environ. 4 (5), 351. https://doi.org/10.1038/s43017022-00378-6, 351.

Shukla, M.K., 2023. Soil Physics: an Introduction. CRC press.

Sippel, S., Meinshausen, N., Fischer, E.M., et al., 2020. Weather variation now detectable from any single day of weather at global scale. Nat. Clim. Change 10, 35–41.

Solari, M.E., 1967. Chakravarti,Im - handbook of methods of applied statistics. Nature 216 (5118), 901. &.

SRAT-TWDB 1999 Comprehensive Sabine Watershed Management Plan, Sabine River Authority of Texas (SRAT) in Conjunction with the Texas Water Development Board (TWDB), Texas.

Trenberth, K.E., 2011. Changes in precipitation with weather variation. Clim. Res. 47 (1–2), 123–138.

Tripathi, R., Sengupta, S.K., Patra, A., Chang, H.J., Jung, I.W., 2014. Weather variation, urban development, and community perception of an extreme flood: a case study of Vernonia, Oregon, USA. Appl. Geogr. 46, 137–146.

Turner, R.E., Rabalais, N.N., 2019. World Seas: an Environmental Evaluation. Elsevier, pp. 445–464.

Turner, R.E., Rabalais, N.N., Alexander, R.B., McIsaac, G., Howarth, R.W., 2007. Characterization of nutrient, organic carbon, and sediment loads and concentrations from the Mississippi River into the Northern gulf of Mexico. Estuaries Coasts 30 (5), 773–790.

Walker, J.F., Hay, L.E., Markstrom, S.L., Dettinger, M.D., 2011. Characterizing weather-change impacts on the 1.5-yr flood flow in selected basins across the United States: a probabilistic approach. Earth Interact. 15.

Wang, L.X., Justic, D., 2009. A modeling study of the physical processes affecting the development of seasonal hypoxia over the inner Louisiana-Texas shelf: circulation and stratification. Cont. Shelf Res. 29 (11–12), 1464–1476.

Wu, C.X., Qiu, D.X., Gao, P., Mu, X.M., Zhao, G.J., 2022. Application of the InVEST model for assessing water yield and its response to precipitation and land use in the Weihe River Basin, China. J Arid Land 14 (4), 426–440.

Wullschleger, S.D., Hanson, P.J., Tschaplinski, T.J., 1998. Whole-plant water flux in understory red maple exposed to altered precipitation regimes. Tree Physiol. 18 (2), 71–79.

Xu, Y.J., Wu, K.S., 2006. Seasonality and interannual variability of freshwater inflow to a large oligohaline estuary in the Northern Gulf of Mexico. Estuar. Coast Shelf Sci. 68 (3–4), 619–626.

Xu, Z., Xu, Y.J., 2018. Assessing effectiveness of long-term forestry best management practices on stream water quality at a basin scale-a case study in Southern USA. Environ. Monit. Assess. 190 (3).